

Functionally graded nanobeams subjected to large deflection by considering surface effects

Yasser Taghipour*, Moslem Zeinali

Department of Mechanical Engineering, Sirjan University of Technology, Sirjan, Iran.

ABSTRACT

In the current study, structurally graded nanobeams with distributed load are subjected to a large deflection analysis that takes surface effects into account. The nanobeams Young's elasticity modulus changes with thickness under a power-law function. The displacement elements are presented, generalization of the Young-Laplace formula is employed to account for the surface effects, and the total Lagrangian finite element formulation is utilized to get the outcomes by cracking the system of nonlinear differential equations founded on the Timoshenko beams theory. The reliability and correctness of the findings are confirmed by comparison with previously published publications. The investigation is done into how various characteristics, including length-to-thickness ratio, material gradient index, boundary conditions, and surface effects, affect the outcomes. The findings demonstrate that, in the presence of surface effects, residual surface tension plays a significant influence on the deflection of nanobeams. Additionally, a comparison of the power-law and exponential kinds of FG distribution is conducted in this study, and it is discovered that the FG materials with the power-law distribution are more applicable since they are less susceptible to surface effects than the exponential type.

Keywords: Nanobeams; Large Deflection; Functionally Graded Materials; Surface Effects; Finite Element Method.

1. Introduction

Functionally graded (FG) materials are one of the motivating constituents of structures for scientists. FG materials are oncoming composites usually produced from two different materials, the first one is a metal with high mechanical stiffness while the second one is a ceramic with high-temperature resistance. In FG materials, properties vary gradually over the volume which notably lets to reduce delamination, stress concentrations, and cracking problems observed in classical composite materials [1-4].

* Corresponding author (Mobile number:, E-mail: ytaghipour@sirjantech.ac.ir)

Various researches on the analysis of FG beams [5-11] and plates [12-21] have been done by many scientists, by the classical theory of elasticity. Here, some of the research on the analysis of FG beams have been mentioned. Benatta et al. [5] constructed the governing equations to assess the behavior of FG short beams under three-point bending using the higher-order shear deformation idea and the idea of virtual work. To illustrate the differences in material qualities, they employed a basic power-law function. Kang and Li [6] examined a cantilever FG beam to comprehend its large deflection behavior. They took into account how the structure's reaction will be affected by the material gradient index. The work by Li et al. [7] discussed the bending study of FG beams utilizing the Timoshenko beam theory (TBT). They acquired the outcomes under various border circumstances. Additionally, Murin et al. [8] reported their research on the modal analysis of FG beams and looked at the impact of the shear correction factor on it in another paper. Sitar et al. research's on the large deformation behavior of FG composite beam is found in [9]. They explored various stress-strain relations in the tension and compression domains under the assumption that the beams are made up of an infinite number of laminates. Concerning tapered FG beams that were subjected to end stresses using the finite element (FE) approach, Kien and Gan [10] produced a significant deflection. The Newton-Raphson iterative approach and the arc-length control algorithm were both used to produce the large deflection response.

In addition to the aforementioned, due to its distinctive features, nanostructure applications are now expanding quickly. Depending on the kind of material utilized, nanostructures like nanobeams and nanoplates may be used in a variety of sectors to make equipment for aerospace, medical, and other fields. The researchers searched for a way to accurately replicate the behavior of the nanostructure since the conventional elasticity theory is unable to account for dimension effects. Based on increasing the surface-to-volume ratio in the nanostructures, modified theories of elasticity by the surface effects are suggested for the modeling the size effects [22].

Various analyses of structures have been conducted by many scientists, based on the theories of elasticity particularly FG structures with surface effects [22-27]. To examine the elastic mechanical behavior of FG films in the nano-dimension, Lü et al. [23] considered surface effects. They offered various numerical examples to determine the impacts of the surface on the bending behavior of the nanostructure mentioned above and employed Kirchhoff's theory, which is often used for thin structures and disregards the impacts of shear deformation. Sharabiani and Yazdi [24] investigated the vibration analysis of FG nanobeams. They used the Euler-Bernoulli theory (EBT) and von Karman nonlinear relations. They studied the

surface influence on the behavior of nanobeams, and they provided the findings for various boundary conditions. In their study [25] on the buckling behavior of FG nanoplates in various shapes, such as elliptical, circular, and skew ones, Ansari et al. considered the surface stress and size impacts. Based on the Eringen and Gurtin-Murdoch hypotheses, they considered size effects. In their research, the Mori-Tanaka homogenization technique was used to ascertain the useful characteristics of the FG nanostructure. Recent research on the use of FE modeling for large deflection analyses of two different kinds of nanobeams was conducted by Taghipour and Baradaran [22]. The first kind of nanobeams was prismatic, whereas the second kind was tapered. They compared their findings to those of experiments and took into account the impact of residual surface stress on the behavior of the nanobeam, as well as the influence of surface through the extended Young-Laplace formula in equations. TBT and nonlocal theory were utilized by Saffari et al. [26] to examine the dynamic stability of FG materials. Based on certain purposes, FG materials' characteristics might vary depending on their thickness or other factors. The characteristics are continuously varied, which is their main specification. Because of their exceptional qualities under various loading situations, their use in many scientific domains is expanding significantly. Saffari et al. [26] evaluated the characteristics of the FG nanostructure over its thickness using a power-law function. To extract the differential equations, they used Hamilton's principle and von Karman's nonlinearity presumptions. The Gurtin-Murdoch continuum theory was also used by them to consider the surface tension impacts. Utilizing three alternate model of beams, Hashemian et al. [27] produced bending and buckling evaluations of nanobeams. The governing equations are developed from nonlocal strain gradient theory that takes surface effects into account. The governing equation is cracked by Navier's method.

In addition to investigating the small deflection of beams with different beam theories [5,7,8,11,27-29], generally, two different types of theory may be used to analyze the large deflection of beams [6,9,10,22,24,26], it has detailed by Taghipour and Darfarin [30]. There are two types of people: the first ignores the shear deformation effect, while the second considers it. EBT for beams is one such theory that typically only takes into account the deformation of thin beams [6,9]. However, TBT behaves differently and takes shear deformations into account, allowing it to be applied to thick beams [10,22]. The nonlinear governing differential equations are extracted founded on TBT, which are more precise in comparison to other cases, even with nonlinear von Karman strains [24,26].

A review of previously published publications in the open literature reveals a lack of research on the large deflection of FG nanobeams that accounts for surface effects, based on TBT. The

goal of the present work is to use the generalization of Young-Laplace equation to investigate the large deflection analysis of FG nanobeams under distributed load and with attention to surface effects. The FG nanobeam's characteristics vary in the thickness direction according to a power-law function that takes into account the gradient index of material in the displayed material distribution. The governing equations are solved using the total Lagrangian FE formulation, which can produce the result for a variety of boundary conditions and loading types. The impact of the most important factors on the dimensionless deflection of the under-considered structure is then taken into account once the findings have been validated against those that have already been published. The findings of this research might be used to design and produce nanostructures with the appropriate qualities to withstand various loading circumstances.

2. Mathematical Formulations

The under-considered models are nanobeams with two different cross-sectional shapes: circular and rectangular cross-sections, as previously mentioned and illustrated in Figure 1. t_l displays the nanobeam thickness for both circular and rectangular shapes. The diameter of the circular type is represented by D , while the height and breadth of the rectangular nanobeam are shown by t and w , respectively. For both kinds, the source of the coordinate system is situated at the center point.

The deflection of the nanobeam, composed of bulk and surfaces and as a result has various characteristics with stress interactions and continuous deformations, is captured by the extended Young-Laplace equation as a modified continuum theory. The surface's overall stress-strain relationship may be expressed as [22]:

$$\tau_{ij} = \tau_{ij}^0 + S_{ijkl} \varepsilon_{kl}, \quad i, j = 1, 2, \quad (1)$$

Where S_{ijkl} is the stiffness tensor, τ_{ij} represents the second-order stress tensor of surface, τ_{ij}^0 is the starting stress of surface, and ε_{kl} is the strain tensor of surface. For the one-dimensional situation of nanobeams, Eq. (1) may be reduced as follows:

$$\tau = \tau_0 + E_s \varepsilon_x, \quad (2)$$

Where E_s is the surface's elasticity modulus and τ_0 is the residual surface stress.

For nanobeams with a high deflection, the distributed load that is parallel to the neutral axis and caused by surface effects is seen in Figure 2 and may be expressed as [22]:

$$q_s = H \kappa_\theta, \quad (3)$$

The constant parameter i.e., H is given by the cross-section type and is equal to $2\tau_0 w$ for a rectangular cross-section and $2\tau_0 D$ for a circular one. κ_θ is the curvature of the neutral axis (i.e., its slope with respect to X), and H is a constant parameter. Figure 3 illustrates the deformation of the cross-section of a nanobeam based on TBT, where the particle P_0 position in the undeformed state becomes P after deformation. As a result, the coordinate of a particle like P in the situation of deformation may be written as [31]:

$$x = X + u_0 - Y \sin \varphi, \quad (4)$$

$$y = v_0 + Y \cos \varphi, \quad (5)$$

The centroid's displacements in the X and Y directions are indicated in the relationships above by u_0 and v_0 , respectively. Additionally, respectively, φ and θ depict the neutral axis slope and cross-section rotation. It should be noted that the shear strain in the section is specified as $(\theta - \varphi)$ based on TBT.

The deformation gradient matrix for the preceding equations (Eqs. (4) and (5)) is [31]:

$$\mathbf{F} = \begin{bmatrix} \frac{\partial x}{\partial X} & \frac{\partial x}{\partial Y} \\ \frac{\partial y}{\partial X} & \frac{\partial y}{\partial Y} \end{bmatrix} = \begin{bmatrix} 1 + u'_0 - Y\kappa_\varphi \cos \varphi & -\sin \varphi \\ v'_0 - Y\kappa_\varphi \sin \varphi & \cos \varphi \end{bmatrix}, \quad (6)$$

Where the prime sign denotes a derivative with regard to X and κ_φ represents the curvature (that is, the derivative of φ).

Utilizing the matrix of deformation gradient as shown below, it is possible to create the green strain matrix [31]:

$$\mathbf{E} = \frac{1}{2}(\mathbf{F}^T \mathbf{F} - \mathbf{I}) = \begin{bmatrix} E_{XX} & E_{XY} \\ E_{YX} & E_{YY} \end{bmatrix}, \quad (7)$$

that identity matrix is shown by \mathbf{I} .

Additionally, the non-zero elements of the Green strain matrix are defined as follows using consistent-linearization methods and small-strain assumptions [31]:

$$E_{XX} = e - Y\kappa_\varphi, \quad E_{XY} = E_{YX} = \gamma/2, \quad (8)$$

where [31] defines the average shear strain (that is γ) as well as the center axial strain (that is e) as follows:

$$e = (1 + u'_0) \cos \varphi + v'_0 \sin \varphi - 1, \quad \gamma = -(1 + u'_0) \sin \varphi + v'_0 \cos \varphi. \quad (9)$$

The prior equations, i.e. (9), showed the nonlinearity of the strains versus displacement

functions. This nonlinearity is geometrical. If the small deflections are considered, it is logical that $\varphi \ll 1$, and the equations convert to linear form, i.e., $e = u'_0$ and $\gamma = -\varphi + v'_0$.

The internal forces N (resulting from axial force), V (resulting from transverse shear force), and M (resulting from bending moment) are calculated by integrating the stress elements [31]:

$$N = \int_{A_0} S_{XX} dA, \quad V = \int_{A_0} S_{XY} dA, \quad M = -\int_{A_0} YS_{XX} dA, \quad (10)$$

where S_{XX} represents the second Piola-Kirchhoff stress under normal conditions, and S_{XY} represents the stress under shear conditions.

In light of this, the vector \mathbf{z} , also known as the general stress resultant vector [31]:

$$\mathbf{z} = [N \quad V \quad M]^T. \quad (11)$$

The general strain vector, in contrast, \mathbf{h} is described as [31]:

$$\mathbf{h} = [e \quad \gamma \quad \kappa_\varphi]^T. \quad (12)$$

To establish the relationship between the general strain vector \mathbf{h} and the stress resultant vector \mathbf{z} , the next equation is used [31]:

$$\mathbf{z} = \mathbf{C} \mathbf{h}, \quad (13)$$

The non-zero components of the constitutive matrix \mathbf{C} are obtained as:

$$C_{11} = b \int_{-h-y_0}^{h-y_0} E(y) dy, \quad C_{22} = \frac{5}{6} \frac{C_{11}}{(2+2\nu)}, \quad C_{33} = b \int_{-h-y_0}^{h-y_0} y^2 E(y) dy, \quad (14)$$

where h , b , and ν represent the structure's half-height, width, and Poisson's ratio. Furthermore, as previously mentioned, the structure's characteristics (that is, Young's elasticity modulus) are functionally graded along its thickness direction, as illustrated in Figure 4, and the next power-law function is taken into account for its fluctuations [32]:

$$E(y) = (E_2 - E_1) \left(\frac{y}{2h} + \frac{1}{2} \right)^n + E_1, \quad (15)$$

Here, n is referred to as the material gradient index of FG materials, which depicts how the material is distributed across the thickness of the construction. Additionally, the structure's top and bottom surfaces' Young's elasticity moduli are E_1 and E_2 , respectively.

The following relation may be used to produce the applied uniform distributed load q :

$$q = Q \frac{C_{33}}{\psi l^3}, \quad (16)$$

where Q stands for the dimensionless evenly distributed load, and l stands for the nanobeam's length. Also:

$$\psi = 1 + \frac{3\left(\frac{E_2}{E_1} - 1\right)(n^2 + n + 2)}{(n+1)(n+2)(n+3)}. \quad (17)$$

3. Total Lagrangian FE Formulation

The prismatic beam element by two end nodes is regarded as having six degrees of freedom (DOF) overall and three DOF at each node in the FE formulation (see Figure 5). The following kinds of assembly are used for this DOF and the associated nodal forces [31]:

$$\mathbf{u} = \begin{bmatrix} u_1 \\ v_1 \\ \varphi_1 \\ u_2 \\ v_2 \\ \varphi_2 \end{bmatrix}, \quad \mathbf{f} = \begin{bmatrix} f_{X1} \\ f_{Y1} \\ M_1 \\ f_{X2} \\ f_{Y2} \\ M_2 \end{bmatrix}, \quad (18)$$

Here, the nodal displacement is \mathbf{u} , and the force vector is \mathbf{f} . Additionally, subscripts 1 and 2 indicate the values of $u_0(X)$, $v_0(X)$, and $\varphi(X)$ at the first and second nodes, respectively. Additionally, the values of the X -component, Y -component, and external bending moment at first (i.e., subscript 1) and second (i.e., subscript 2) nodes are indicated by the variables f_{xi} , f_{yi} , and M_i ($i=1, 2$).

The following relation may be used to represent fluctuations in internal energy with regard to nodal displacements [31]:

$$\delta U = \mathbf{p}^T \delta \mathbf{u}, \quad (19)$$

where \mathbf{p} is the internal force vector with the following definition [31]:

$$\mathbf{p} = \int_{L_0} \mathbf{B}^T \mathbf{z} d\bar{X}. \quad (20)$$

By using the nodal displacement vector \mathbf{u} together with Lagrangian shape functions, considering the partial derivatives of e , γ , and κ_φ , and then rewriting $u_0(X)$, $v_0(X)$, and $\varphi(X)$, we may derive \mathbf{B} as follows [31]:

$$\mathbf{B} = \frac{1}{L_0} \begin{bmatrix} -\cos \varphi & -\sin \varphi & L_0 N_1 \gamma & \cos \varphi & \sin \varphi & L_0 N_2 \gamma \\ \cos \varphi & -\cos \varphi & -L_0 N_1 (1+e) & -\cos \varphi & \cos \varphi & -L_0 N_2 (1+e) \\ 0 & 0 & -1 & 0 & 0 & 1 \end{bmatrix}, \quad (21)$$

where L_0 represents the element's original length before deformation and:

$$N_1 = (1 - \xi) / 2, \quad N_2 = (1 + \xi) / 2, \quad (22)$$

Here, ξ is the element's natural coordinate, which is between -1 and $+1$, and is denoted by the symbol. The generalized displacement vector's increment, denoted by the symbol $\delta \mathbf{u}$, is determined for each iteration as follows [31]:

$$\delta \mathbf{u} = \mathbf{K}^{-1} \delta \mathbf{p}, \quad (23)$$

$\delta \mathbf{h} = \mathbf{B} \delta \mathbf{u}$ is taken into consideration, the initial variants of \mathbf{z} and \mathbf{B} are used, and \mathbf{K} is the tangent stiffness matrix whose components may be calculated employing Eqs. (12) and (13). As a result, incremental Eq. (23) may be represented using the iteration form below [22]:

$$\mathbf{u}^{(r+1)} = \mathbf{u}^{(r)} + \left[\mathbf{K}^{(r)} \right]^{-1} \left(\mathbf{p}^{(r+1)} - \mathbf{p}^{(r)} \right), \quad (24)$$

that r displays the number of iterations. The loads are exerted in a series of steps as [22]:

$$\mathbf{p}^{(r+1)} = \mathbf{f}_e^{(r)} + \mathbf{f}_s^{(r)}, \quad (25)$$

In Eq. (25), the force vector $\mathbf{f}_e^{(r)}$ that results from the external loads and the force vector $\mathbf{f}_s^{(r)}$ resulting from the dispersed load (i.e., q_s) are both stated.

In each phase, $\mathbf{f}_e^{(r)}$ is also determined based on the external loads, and it is important to highlight that it is a conservative load. It should be noted that there have been no modifications to any of the steps' iterations.

However, since $\mathbf{f}_s^{(r)}$ is caused by a non-conservative load (q_s), its specifications (i.e., direction and magnitude) are altered by a change in the elements of the nodal displacement vector.

Thus, $\mathbf{f}_s^{(r)}$ is modified after each repetition. In the first iteration of the first load step, \mathbf{u}^1 is set to be a zero vector, leading to the production of \mathbf{p}^1 and \mathbf{f}_s^1 . The subsequent repetitions are repeated until each load step has the required precision [22].

4. Results and Discussion

4.1. Validation Study

To assure the trustworthiness and correctness of the findings, a comparison between the most recent results and those that have already been published is made before the results are shown. To this goal, the authors omitted several criteria to make the findings compared to other works since the current study is the first analysis with the requirements mentioned above, and there is not a similar one in the literature to compare the results with.

Accordingly, the dimensionless deflections are produced for various l/h ratios and compared with the present ones in Figure 6 with respect to Li et al. study [7], which is about an FG macro beam with both ends clamped condition. Without surface effects and with $n=2$, the findings in Figure 6 were achieved. Additionally, in this scenario, the beam is under a

uniformly distributed load ($Q=I$). Additionally, the top and bottom surfaces' Young's elasticity moduli are estimated to be 70 GPa and 380 GPa, respectively, with a Poisson's ratio of 0.23.

It can be shown that the findings for various length-to-thickness ratios (i.e., l/h) are in excellent agreement with one another, with a small amount of variation perhaps arising from the use of different beam theories in Li et al. [7] investigation or alternative approaches to problem-solving. As a result, it is guaranteed that the formulations, solution process, and programmed code are correct. The findings of this investigation are therefore described in the paragraphs that follow.

4.2. Case Study

The findings of the current effort are now shown by guaranteeing their dependability in a more straightforward form. Thus, the results are derived for various boundary conditions using the aforementioned material characteristics and taking surface effects into account. The beam has a rectangular cross-sectional area that is 100 nanometers wide and 1000 nanometers long.

Figure 7 and Figure 8 show, in the contexts of both ends, clamped and simply supported, respectively, how surface stresses affect the dimensionless deflection of the nanobeam. As shown in Figure 7, the impact of surface stresses on the deflection of the nanobeam may vary depending on the value of τ_0 (i.e., residual surface stress, which can be either positive or negative).

Considered to be 0.28 nN/nm and 1.52 nN/nm for the top and bottom surfaces, respectively, in Figure 7, it can be observed that accounting for surface effects causes the deflection to decrease. Additionally, it can be inferred that when negative values for τ_0 are taken into account, the dimensionless deflection of the nanobeam behaves differently, i.e., taking into account surface effects increased the deflection of the structures.

Figure 8 depicts a distinct outcome, but for both ends, a straightforward supported nanobeam. As can be observed, capturing surface effects, with a positive value for τ_0 , causes the dimensionless deflection to decrease, and raising the l/h ratio causes the nanobeam's deflection to decrease. This figure is presented for two values of l/h , which is a criterion of nanobeam thickness.

The dimensionless deflection of a cantilever nanobeam with a positive value for τ_0 is shown in Figure 9. As is seen from Figure 9, incorporating surface effects with negative values of τ_0 leads to an increase in the structure's deflection. In other words, the direction of the

distributed loads caused by surface effects and the direction of the distributed external load is aligned in this picture, increasing the deflection.

Figure 10 shows the impact of the material gradient index n on the dimensionless deflection of the FG nanobeam. The stiffness of the whole structure decreases when the material gradient index is raised because the characteristics of the nanobeam vary from stiffer to softer places. As a result, the nanobeam's deflection improves. Positive residual surface stress levels are shown at Figure 10, which causes the findings to decrease when surface effects are taken into account.

The power-law distribution, which complies with Eq. (15), is contrasted with the exponential kind of property distribution, which complies with the following function, to assess how the two types of material properties distribution affect the outcomes.

$$E(y) = E_2 e^{\left(\frac{1}{2h}\right) \ln\left(\frac{E_1}{E_2}\right)(y+h)}, \quad (26)$$

The two forms of distribution are compared in Figure 11, and it is clear that although the overall behavior of the structure in both types is similar, the results based on the power-law function are fewer than those based on the exponential function. It should be mentioned that $n=2$ and a cantilever nanobeam were used to get the findings in Figure 11.

5. Conclusions

The current study presents a large deflection analysis of an FG nanobeam, taking surface effects into account. A power-law distribution governs how the Young's elasticity modulus changes with thickness of the nanobeam. The generalized Young-Laplace equation accounts for the surface effects, and the displacement elements are added founded on TBT, which also accounts for the shear deformation effects. The nonlinear differential equations are cracked using the total Lagrangian FE formulation, and the outcomes are confirmed using earlier published research in the simpler state [22]. The impact of various factors on the results is taken into account for various boundary conditions to ensure the accuracy of the findings, and it is seen that the sign of residual surface stress plays a significant influence on the deflection of the nanobeam. In other words, aimed at simply supported conditions, for residual surface stress values that are positive, considering surface effects causes the deflection to decrease, but for residual surface stress values that are negative, including surface effects causes the deflection to increase, and vice versa aimed at clamped supported conditions. Additionally, when the l/h ratio rises, which is a need for nanobeam thickness in all boundary types taken into consideration, the deflection decreases, and the stiffness of the nanobeam increases.

Increasing the material gradient index n , which depicts the material distribution in the thickness direction, results in a softer structure and, as a result, increases deflection. A comparison between the power-law and exponential forms of FG distribution is conducted to reinforce the originality and thoroughness of this work. According to the findings of contrasting the deflection of power-law and exponential distributions of material kinds, it can be concluded that generally speaking, under the same loading and boundary circumstances, the exponential FG type exhibits a greater deflection than the power-law type. Additionally, power-law models are more helpful since surface effects on the deflection of this FG distribution type are less significant.

Declaration of Conflicting Interests

The authors say they have no competing interests.

References

- [1] Ebrahimi, F. ed. “Mechanics of Functionally Graded Materials and Structures”, *BoD-Books on Demand* (2020).
- [2] Mohammadi, M., Rajabi, M. and Ghadiri, M. “Functionally graded materials (FGMs): A review of classifications, fabrication methods and their applications”, *Process. Appl. Ceram.*, **15**(4), pp. 319-343 (2021).
- [3] Panchal, Y. and Ponappa, K. “Functionally graded materials: A review of computational materials science algorithms, production techniques, and their biomedical applications”, *Proc. Inst. Mech. Eng. C: J. Mech. Eng. Sci.*, **236**(22), pp. 10969-10986 (2022).
- [4] Babaei, M., Kiarasi, F., Asemi, K. and et al. “Functionally graded saturated porous structures: A review”, *J. Comput. Appl. Mech.*, **53**(2), pp. 297-308 (2022).
- [5] Benatta, M.A., Mechab, I., Tounsi, A. and et al. “Static analysis of functionally graded short beams including warping and shear deformation effects”, *Comput. Mater. Sci.*, **44**, pp. 765-773 (2008).
- [6] Kang, Y.A. and Li, X.F. “Large deflections of a non-linear cantilever functionally graded beam”, *J. Reinf. Plast. Compos.*, **29**, pp. 1761-1774 (2010).
- [7] Li, S.R., Cao, D.F. and Wan, Z.Q. “Bending solutions of FGM Timoshenko beams from those of the homogenous Euler-Bernoulli beams”, *Appl. Math. Model.*, **37**, pp. 7077-7085 (2013).
- [8] Murin, J., Aminbaghai, M., Hrabovský, J. and et al. “Modal analysis of the FGM

- beams with effect of the shear correction function”, *Compos. B.: Eng.*, **45**, pp. 1575-1582 (2013).
- [9] Sitar, M., Kosel, F. and Brojan, M. “Large deflections of nonlinearly elastic functionally graded composite beams”, *Arch. Civ. Mech. Eng.*, **14**, pp. 700-709 (2014).
- [10] Kien, N.D., and Gan, B.S. “Large deflections of tapered functionally graded beams subjected to end forces”, *Appl. Math. Model.*, **38**, pp. 3054-3066 (2014).
- [11] Sahu, R., Sutar, M. and Pattnaik, S., “A generalized finite element approach to the free vibration analysis of non-uniform axially functionally graded beam”, *Sci. Iran.*, **29**(2), pp. 556-571 (2022).
- [12] Reddy, J.N. “Analysis of functionally graded plates”, *Int. J. Numer. Methods Eng.*, **47**, pp. 663-684 (2000).
- [13] Ghannadpour, S.A.M. and Alinia, M.M. “Large deflection behavior of functionally graded plates under pressure loads”, *Compos. Struct.*, **75**, pp. 67-71 (2006).
- [14] Ovesy, H.R., and Ghannadpour, S.A.M. “Large deflection finite strip analysis of functionally graded plates under pressure loads”, *Int. J. Struct. Stab. Dyn.*, **7**, pp. 193-211 (2007).
- [15] Chung, Y.L. and Chen, W.T. “Bending behavior of FGM-coated and FGM-undercoated plates with two simply supported opposite edges and two free edges”, *Compos. Struct.*, **81**, pp. 157-167 (2007).
- [16] Khabbaz, R.S., Manshadi, B.D. and Abedian, A. “Nonlinear analysis of FGM plates under pressure loads using the higher-order shear deformation theories”, *Compos. Struct.*, **89**, pp. 333-344 (2009).
- [17] Parida, S. and Mohanty, S. “Nonlinear free vibration analysis of functionally graded plate resting on elastic foundation in thermal environment using higher order shear deformation theory”, *Sci. Iran.*, **26**(2), pp. 815-833 (2019).
- [18] Phuong, H.T., Quoc, T.H. and Hien, H.T. “Static analysis of four-parameter functionally graded plates with general boundary conditions”, *J. Sci. Technol. Civ. Eng. (STCE)-HUCE.*, **13**(2), pp. 12-23 (2019).
- [19] Kumar, P. and Harsha, S.P. “Modal analysis of functionally graded piezoelectric material plates”, *Mater. Today: Proc.*, **28**(3), pp. 1481-1486 (2020).
- [20] Toudehdeghan, A. “Static analysis of functionally graded coated plate on elastic foundation based on Levy method”, *IOP Conf. Ser.: Mater. Sci. Eng.*, **854**(012036), pp. 1-10 (2020).
- [21] Ramteke, P., Mehar, K., Sharma, N. and et al. “Numerical prediction of deflection and

- stress responses of functionally graded structure for grading patterns (power-law, sigmoid, and exponential) and variable porosity (even/uneven)", *Sci. Iran.*, **28**(2), pp. 811-829 (2021).
- [22] Taghipour, Y. and Baradaran, G.H. "A finite element modeling for large deflection analysis of uniform and tapered nanobeams with good interpretation of experimental results", *Int. J. Mech. Sci.*, **114**, pp. 111-119 (2016).
- [23] Lü, C.F., Chen, W.Q. and Lim, C.W. "Elastic mechanical behavior of nano-scaled FGM films incorporating surface energies", *Compos. Sci. Technol.*, **69**, pp. 1124-1130 (2009).
- [24] Sharabiani, P.A. and Yazdi, M.R.H. "Nonlinear free vibrations of functionally graded nanobeams with surface effects", *Compos. B: Eng.*, **45**, pp. 581-586 (2013).
- [25] Ansari, R. and Norouzzadeh, A., "Nonlocal and surface effects on the buckling behavior of functionally graded nanoplates: An isogeometric analysis", *Phys. E Low-Dimensional Syst. Nanostructures*, **84**, pp. 84-97 (2016).
- [26] Saffari, S., Hashemian, M. and Toghraie, D. "Dynamic stability of functionally graded nanobeam based on nonlocal Timoshenko theory considering surface effects", *Phys. B Condens. Matter.*, **520**, pp. 97-105 (2017).
- [27] Hashemian, M., Foroutan, S. and Toghraie, D. "Comprehensive beam models for buckling and bending behavior of simple nanobeam based on nonlocal strain gradient theory and surface effects", *Mech. Mater.*, **139**, pp.1-11 (2019).
- [28] Haddad, S., Baghani, M. and Zakerzadeh, M. "Size dependent analysis of tapered FG micro-bridge based on a 3D beam theory", *Sci. Iran.*, **27**(6), pp. 2889-2901 (2020).
- [29] Gholami, M. and Alizadeh, M. "A quasi-3D modified strain gradient formulation for static bending of functionally graded micro beams resting on Winkler-Pasternak elastic foundation", *Sci. Iran.*, **29**(1), pp. 26-40 (2022).
- [30] Taghipour, Y. and Darfarin, S. "A method for comparison of large deflection in beams", *Int. J. Appl. Mech. Eng.*, **27**(4), pp. 179-193 (2022).
- [31] Felippa, C.A. "Nonlinear finite element methods", *As. Eng. Sci. Dept. Cu. Boulder* (2001).
- [32] Arshid, E., Kiani, A., and Amir, S. "Magneto-electro-elastic vibration of moderately thick FG annular plates subjected to multi physical loads in thermal environment using GDQ method by considering neutral surface", *Proc. Inst. Mech. Eng. L: J. Mater.: Des. Appl.*, **233**, pp. 2140-59 (2019).

Biographies

Moslem Zeinali has a Master's degree in Mechanics from Sirjan University of Technology, Iran 2020. He received his bachelor's degree from Shahid Bahonar University of Kerman in Mechanical Engineering (Solid Mechanics) in 2008. He works for NICICO (National Iranian Copper Industries Company) since 14 years ago. Now he is the head of the Technical and Design office of Sarcheshme copper complex development deputy.

Yasser Taghipour is an Assistant Professor in the Mechanical Engineering Department at Sirjan University of Technology, Iran. He studied in the field of Applied Design (Solid Mechanics) in the Mechanical Engineering. He received his bachelor's degree in 2002 from the Shahid Bahonar University of Kerman, his master's degree in 2004 from Tehran University and his Ph.D. in 2017 from Shahid Bahonar University of Kerman. His research field is Computational Methods in Solid Mechanics. One of the topics of interest is the bending analysis of beams with Surface Effects and Non-local theory based on the Finite Element Method. Recently, he is also researching on optimization methods.

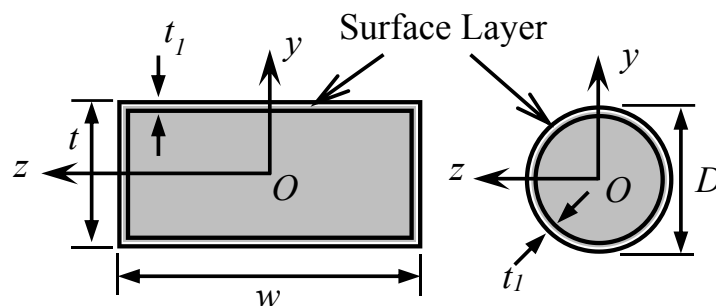


Figure 1. The nanobeam is in two rectangular and circular examples, shown from the cross-section.

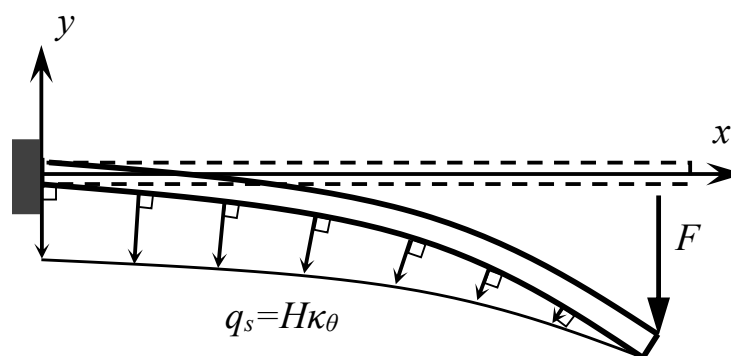


Figure 2. Owing to the positive residual surface stress, distributed load.

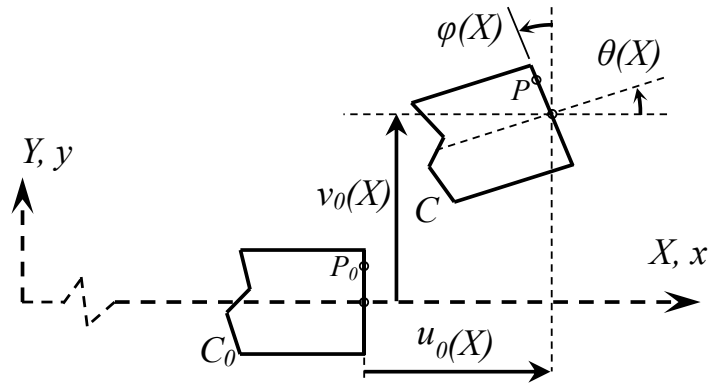


Figure 3. Sectional Timoshenko beam model deformation.

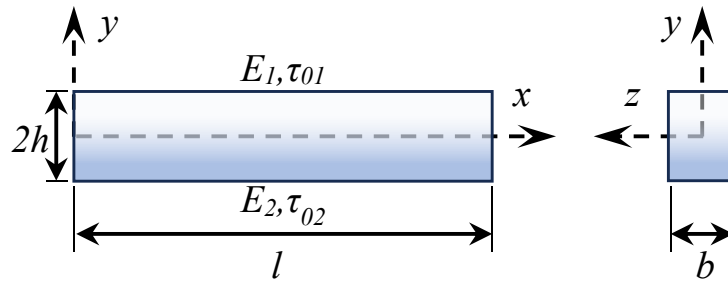


Figure 4. Schematic of FG nanobeam and properties gradient.

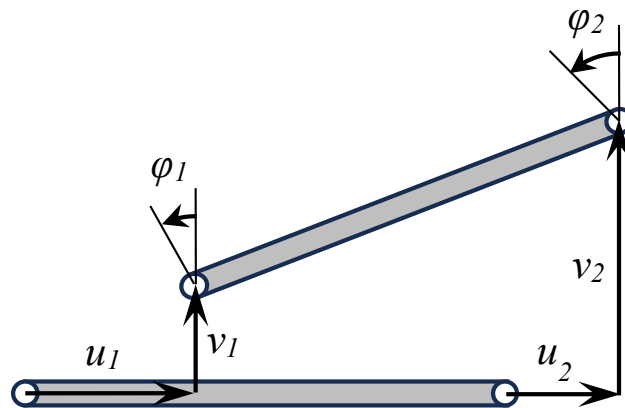


Figure 5. The original and current arrangements of the six degrees of freedom straight linear beam element.

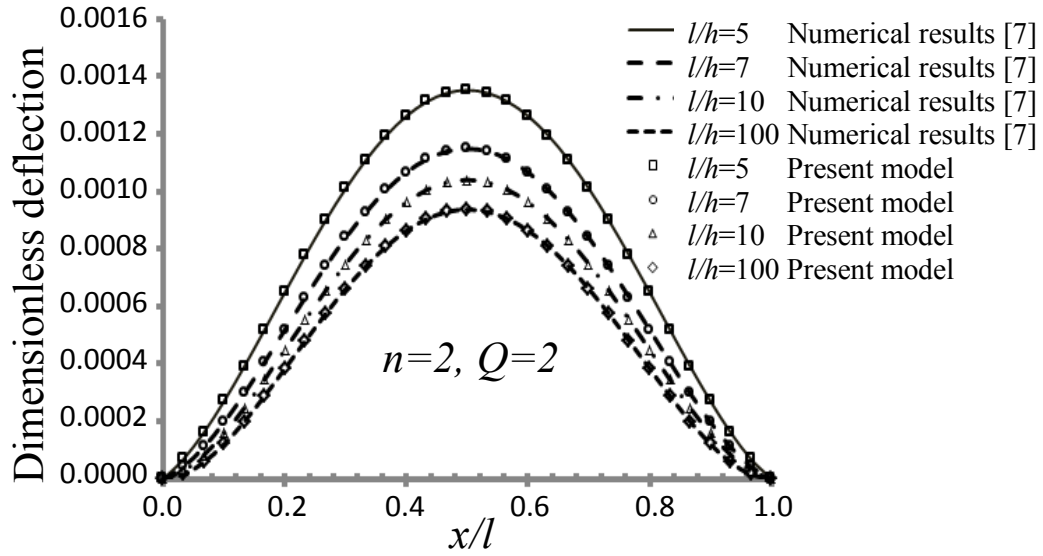


Figure 6. Contrasting macro beam's dimensionless deflection with those of Li et al. [7].

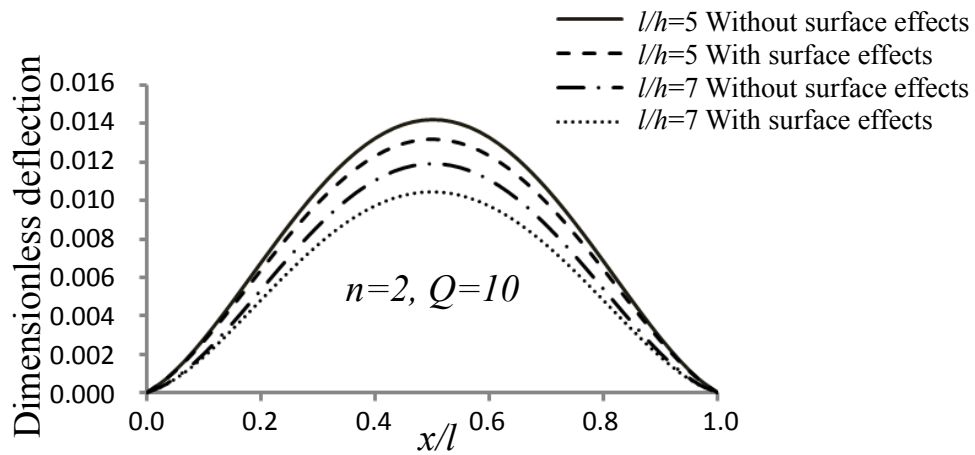


Figure 7. Effects of surface tension and length-to-thickness ratio on the deflection of a nanobeam clamped at both ends.

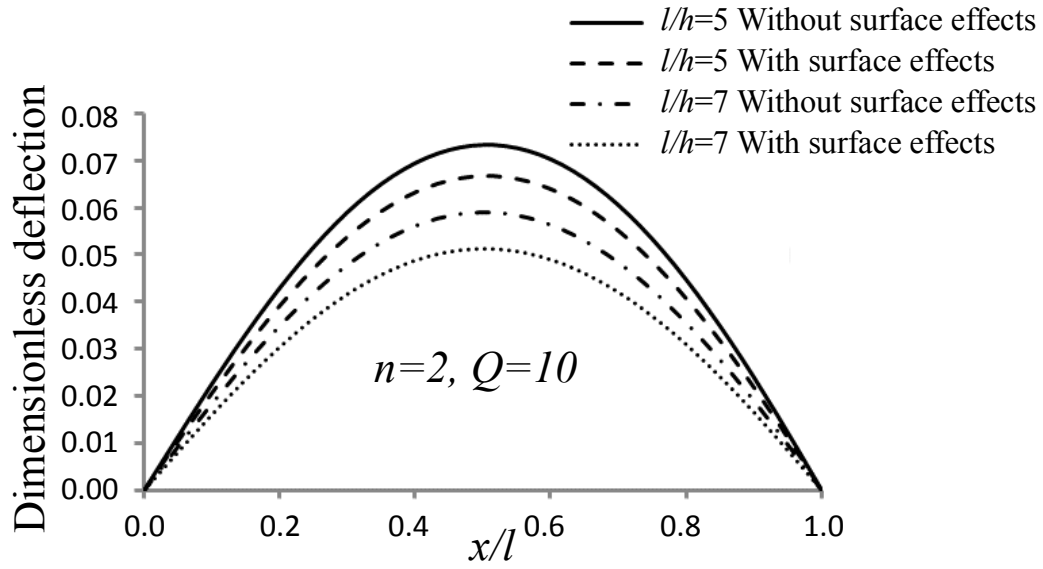


Figure 8. Nanobeam was just supported by the length-to-thickness ratio and surface effects on the deflection of both ends.

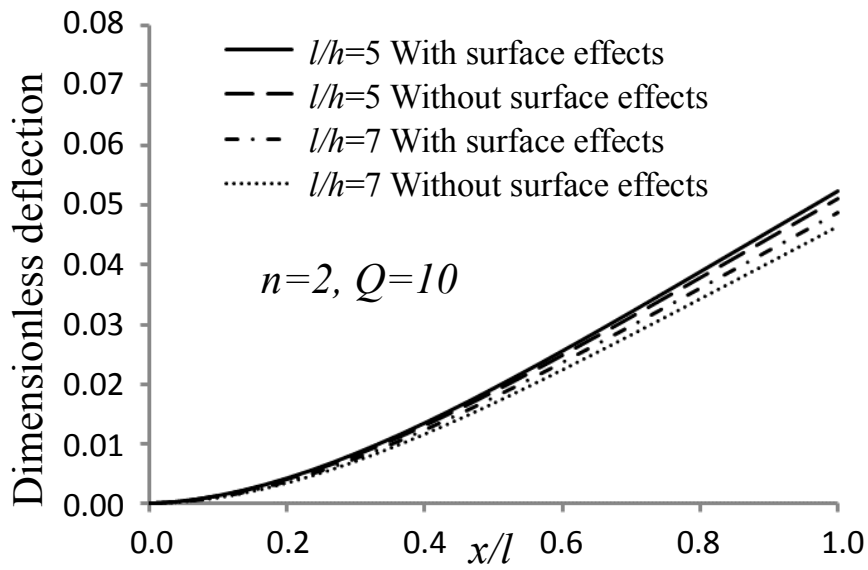


Figure 9. Surface effects and length-to-thickness ratio on cantilever nanobeam deflection.

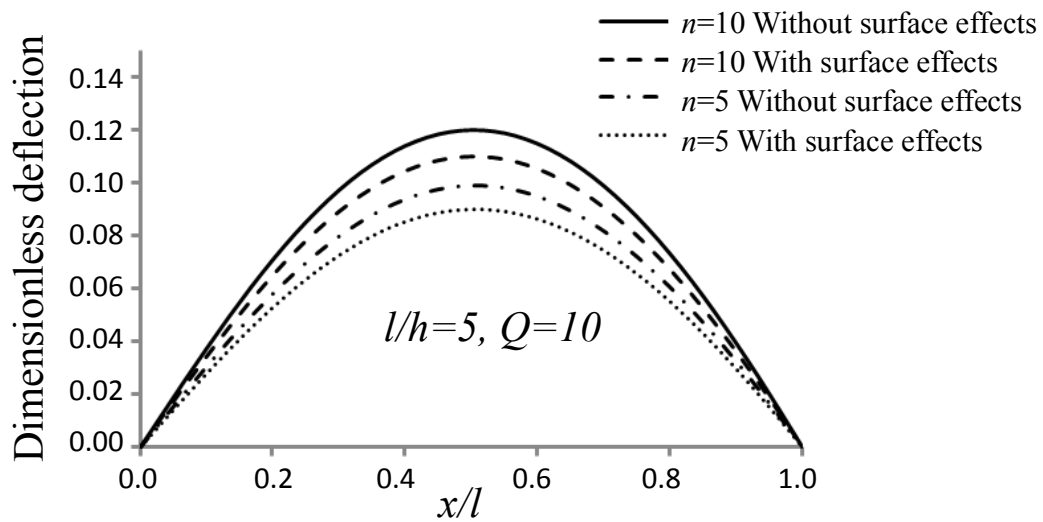


Figure 10. Dimensionless deflection of the nanobeam and the material gradient index of FG materials.

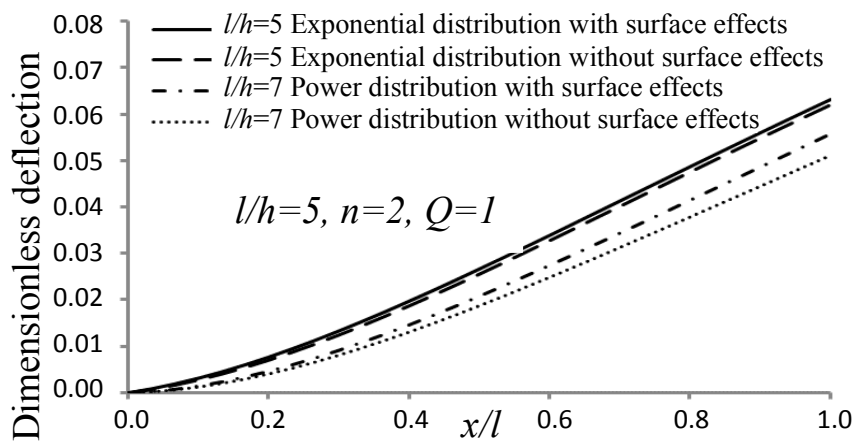


Figure 11. Comparing the outcomes for FG materials with power-law and exponential distribution types.